FULL PAPER

Role of Molecular Sieves in the CVD Synthesis of Large-Area 2D MoTe$_2$

Lin Zhou, Kai Xu, Ahmad Zubair, Xu Zhang, Fangping Ouyang, Tomás Palacios, Mildred S. Dresselhaus, Yongfeng Li,* and Jing Kong*

The synthesis of high-quality 2D MoTe$_2$ with a desired phase on SiO$_2$/Si substrate is crucial to its diverse applications. A side reaction of Te with the substrate Si leading to SiTe and Si$_2$Te$_3$ tends to happen during growth, resulting in the failure to obtain MoTe$_2$. It has been found that molecular sieves can adsorb the silicon telluride byproducts and eliminate the influence of the side reaction during the chemical vapor deposition synthesis of MoTe$_2$. With the help of molecular sieves, few-layer 1T′ MoTe$_2$ can be grown from the MoO$_x$ precursor. Pure 1T′ MoTe$_2$ and 2H MoTe$_2$ regions in centimeter-sized areas synthesized on the same piece of SiO$_2$/Si substrate can be obtained by using an overlapped geometry. The strategy provides a new method to controllably synthesize MoTe$_2$ with desired phases and can be generalizable to the synthesis of other tellurium-based layered materials.

1. Introduction

2D layered materials possess unique structures in which atomic planes of covalently bonded atoms are stacked vertically with only weak van der Waals interactions between the planes.[1,2] Such materials have attracted much attention in recent years because their monolayers or few layers can be isolated into 2D or quasi-2D systems, which have demonstrated very interesting and distinct properties compared to their bulk counterparts.[3–6]

Dr. L. Zhou, Dr. K. Xu, A. Zubair, X. Zhang,
Prof. F. Ouyang, Prof. T. Palacios,
Prof. M. S. Dresselhaus, Prof. J. Kong
Department of Electrical Engineering
and Computer Sciences
Massachusetts Institute of Technology
Cambridge, MA 02139, USA
E-mail: jingkong@mit.edu
Dr. K. Xu, Prof. Y. Li
State Key Laboratory of Heavy Oil Processing
China University of Petroleum
Beijing 102249, China
E-mail: yfli@cup.edu.cn
Prof. F. Ouyang
School of Physics and Electronics, and Institute of Super-Microstructure
and Ultrafast Process in Advanced Materials
Central South University
Changsha 410083, China
Prof. M. S. Dresselhaus
Department of Physics
Massachusetts Institute of Technology
Cambridge, MA 02139, USA

In this family, thin layers of transition metal dichalcogenides (TMDs) with the formula MX$_2$ (M = transition metal of group 4–10; X = S, Se, or Te) are particularly attractive for optoelectronics applications.[7,8] For example, several bulk TMDs are indirect bandgap semiconductors, but will become direct bandgap semiconductors in their monolayer limit.[9,10] Owing to the strong spin-orbit coupling, tellurium-based TMDs, such as WTe$_2$ and MoTe$_2$, have demonstrated some special desirable characteristics. For example, an extraordinarily large magnetoresistance effect was recently found in WTe$_2$, which is quite promising for applications of nanostructured magnetic devices.[11]

Another very interesting finding is that TMDs always have more than one crystal structure with important application potentials.[12,13] In the case of MoTe$_2$, 2H MoTe$_2$ has a trigonal prismatic structure. Because of its bandgap (monolayer and bilayer 2H MoTe$_2$ are direct bandgap semiconductors with bandgaps close to the bandgap of Si),[14] strong absorption throughout the solar spectrum,[15] and strong spin-orbit coupling,[16,17] 2H MoTe$_2$ has been actively investigated for applications in electronics, optoelectronics, spintronics, and photovoltaics.[5,18,19] 1T′ MoTe$_2$ (having a distorted octahedral structure) is metallic, which has the potential to be used for topological quantum spin Hall insulators.[5] The ground-state energy difference between the two crystal structures (1T′ and 2H) is quite small (<0.1 eV).[12] Therefore, a special feature of MoTe$_2$ is that its 1T′ and 2H phases easily coexist under normal conditions. The combination of the 2H and 1T′ MoTe$_2$ heterophase structures could therefore lead to a stable 2D ohmic contact, which may be a significant advantage for MoTe$_2$-based electronic devices.[20] Thus, it is highly desirable to controllably synthesize MoTe$_2$ with different phases.

SiO$_2$/Si substrate has been the most commonly used substrate for the synthesis and investigations of nanomaterials. Particularly for the growth and transfer of 2D materials, on one hand, having the SiO$_2$ with particular thicknesses (e.g., 90 or 300 nm) greatly facilitates the recognition of the presence and even the thicknesses of the 2D materials (light interference causes sufficient optical contrast in the visible regime).[21,22] On the other hand, this allows their straightforward integration, and all the presently used device fabrication techniques in the semiconductor industry can be easily carried out on these hybrid structures. Several methods have been developed to

FULL PAPER

Figure 1. a) A schematic illustration of the sample geometry on the crucible with molecular sieves and Te powder during the MoTe$_2$ CVD process. The small white pellets represent molecular sieves. b) Temperature-controlled sequence used for a typical growth of MoTe$_2$. c) A photograph of the CVD furnace; the red circle region shows the downstream of the gas flow, where the Te begins to condense due to the low temperature of the furnace edge. d) Photograph of the quartz tube with Te and Si$_2$Te$_3$ after the CVD growth when molecular sieves were not used during the synthesis. e) When molecular sieves are introduced into the CVD system, only Te deposition can be found on the quartz tube.

successfully grow 2D TMDs, such as MoS$_2$, MoSe$_2$, WS$_2$, and WSe$_2$, on SiO$_2$/Si substrates.[23–27] The SiO$_2$/Si substrates are stable under the growth conditions (elevated temperatures of 600–1000 °C in the presence of various chemical species). In our study of the MoTe$_2$ synthesis using the chemical vapor deposition (CVD) method, we also used SiO$_2$/Si substrates. It was found that a side reaction of Te with the substrate Si leading to SiTe and Si$_2$Te$_3$[28] tends to happen, resulting in the failure to obtain MoTe$_2$. Such a side reaction could hamper the synthesis of other telluride-based TMDs (such as WTe$_2$, GaTe) as well. Therefore, it is crucial to explore a strategy for the synthesis of high-quality 2D telluride materials with a desired phase on SiO$_2$/Si substrate, and at the same time for suppressing the side reaction between Si and Te.

In this work, we report our findings of the controlled synthesis of MoTe$_2$ using molecular sieves. We have found that by introducing molecular sieves into the CVD system, the side reaction that generates SiTe and Si$_2$Te$_3$ is restrained and few-layer MoTe$_2$ materials could be successfully synthesized on the SiO$_2$/Si substrates. After the CVD growth, Si$_2$Te$_3$ was found to form on the molecular sieves instead of the SiO$_2$/Si growth substrates. It is likely that the molecular sieves adsorb and trap the precursor of the byproduct (SiTe and Te) to facilitate the growth of MoTe$_2$. Both few-layer 1T' MoTe$_2$ and 2H MoTe$_2$ over square centimeter areas were successfully synthesized on the same SiO$_2$/Si substrate. We anticipate that this strategy can be very useful for the synthesis of other 2D telluride materials as well.

2. Results and Discussion

MoTe$_2$ films were synthesized via CVD inside a furnace with a 1 in. diameter quartz tube. A Mo precursor was first deposited on a 300 nm SiO$_2$/Si substrate via thermal evaporation of MoO$_3$ powder. Since MoO$_3$ tends to lose oxygen by evaporation, the resulting precursor is more accurately described as MoO$_x$ ($x < 3$) (thickness: 0.5–2 nm).[29] About 180 mg tellurium (Te, 99.997%; Sigma Aldrich) powder was filled in a crucible. Molecular sieves (29 mg, Na$_{12}$[(AlO$_2$)$_{12}$(SiO$_2$)$_{12}$]· x H$_2$O, 4 Å, Sigma-Aldrich) were mixed with the Te powder in the crucible. The MoO$_x$/SiO$_2$/Si sample was then placed onto the top of the crucible, either facing up or facing down (similar results were obtained, and this geometry is referred to as "the uncovered geometry"). For the study of SiTe and Si$_2$Te$_3$ formation, we also used another substrate geometry, i.e., placing two MoO$_x$/SiO$_2$/Si samples onto the top of the crucible, with one piece having the MoO$_x$ layer facing up, and a portion of its surface covered by the other piece (MoO$_x$ layer facing down), as shown in **Figure 1**a. The MoO$_x$/SiO$_2$/Si samples together with the crucible were loaded into a quartz tube and heated up to 700 °C at a rate of 45 °C min^{-1}, and kept at 700 °C for 60 min in a mixture of 3 sccm Ar and 4 sccm H$_2$ gas. After the growth, samples were first cooled down to 650 °C, then quickly cooled down to room temperature (Figure 1b).

To illustrate the effects of the molecular sieves, controlled experiments were carried out for the CVD growth with and without molecular sieves. The MoO$_x$/SiO$_2$/Si samples were placed on top of the crucible, either with just one substrate in the uncovered geometry (here, sample 2 or 4 represents the typical result of samples without and with molecular sieves, respectively), or with two substrates in the overlapped geometry as shown in Figure 1a; the growth results of the two overlapped pieces were found to be the same, therefore, the result of only one of them is shown. Sample 1 or 3 represents the results of without and with molecular sieves, respectively. The optical microscope images of samples 1–4 are shown in **Figure 2**a. For samples 1 and 2, which were grown without molecular sieves, no MoTe$_2$ was found on the surface after the CVD growth.
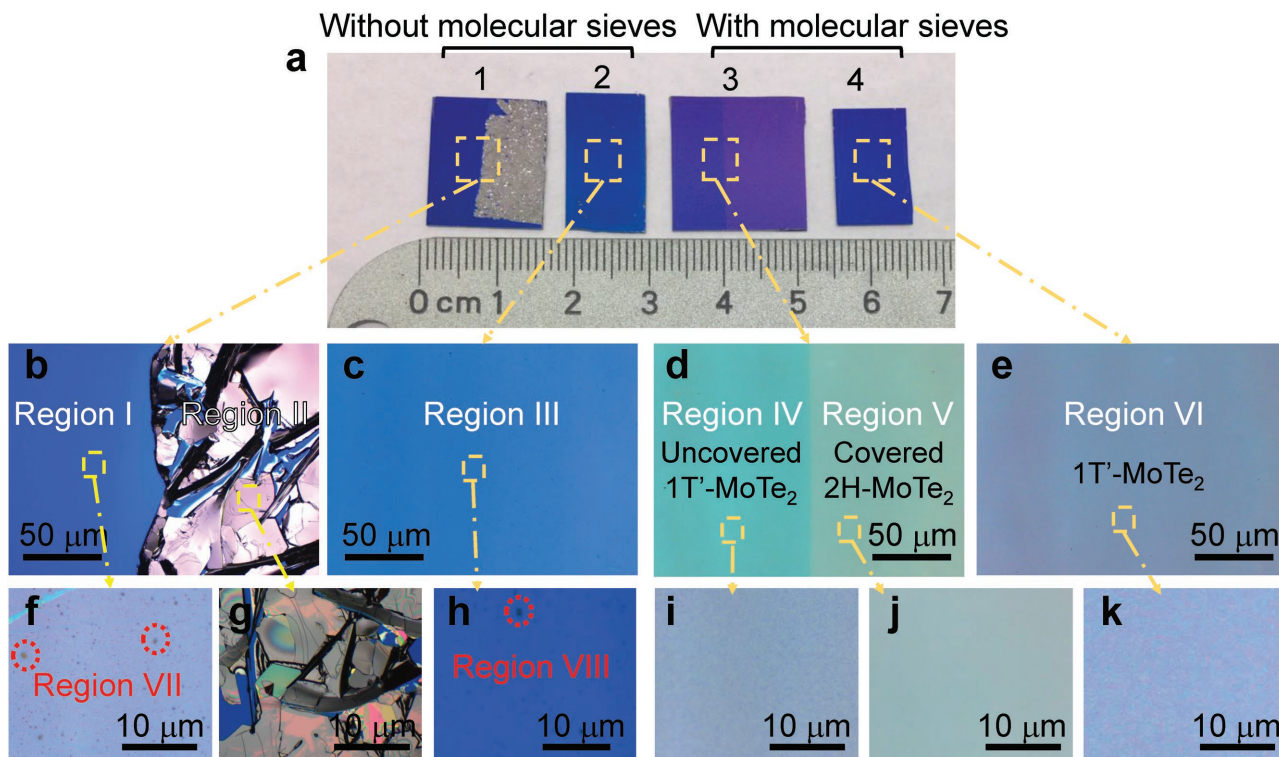
Figure 2. Four samples synthesized with/without molecular sieves under otherwise identical conditions. a) Photograph of the four representative samples. Samples 1 and 2 were synthesized without molecular sieves, and samples 3 and 4 were synthesized with molecular sieves. Samples 1 and 3 were grown using the overlapped geometry, and samples 2 and 4 were grown using the uncovered geometry. b–k) Optical microscope images of different regions on these four samples.

However, with the presence of molecular sieves, both 1T′ (sample 4) and 2H MoTe$_2$ (right-hand side region of sample 3) were obtained.

The side reaction between Si and Te at high temperature sheds light on the phenomena occurring in samples 1 and 2. Without the molecular sieves, it appears that the side reaction dominates and the red products of Si$_2$Te$_3$ were found in the reactor, especially on the edges of substrates and on the inner wall of the quartz tube around the edge of the heating zone (Figure 1d; these can be seen with the naked eye). In addition, for the overlapped sample, Figure 2b shows the optical microscope image of the boundary region between the uncovered side (on the left, region I) and the covered side (on the right, region II). The red sheen color also reveals the presence of Si$_2$Te$_3$ here. For region I, some red particles were also identified on the surface (labelled as Region VII) (Figure 2f). By contrast, there is no red Si$_2$Te$_3$ on either sample or on the quartz tube when molecular sieves were used during the CVD growth (Figures 1e and 2d,e,i,k).

Raman spectroscopy with a 532 nm laser was utilized to characterize the red shining material (Region II) in sample 1 (**Figure 3**a). There is a strong A$_{1g}$ peak at 137 cm^{-1} associated with a small peak at 118 cm^{-1}, a relatively weak E$_g$ peak at 474 cm^{-1}, and a small E$_g$ peak around 326 cm^{-1}, respectively. These peaks are consistent with characteristic peaks of Si$_2$Te$_3$.[28] No MoTe$_2$-related Raman peaks were found in the spectra taken for this region. The possible origin of the Si$_2$Te$_3$ is that the Si from the SiO$_2$/Si substrate can react with Te, which,

in our experiments, appears to become the dominant reaction, preventing MoO$_x$ to react with Te, and thus no MoTe$_2$ could be found. Tellurium vaporizes at a relatively low temperature (T_m = 450 °C) and transports as Te$_2$ vapor. The main source of Si may come from exposed Si at the edge of the SiO$_2$/Si substrate when a wafer was cut into pieces. Though Si does not appreciably vaporize under atmosphere pressures at 700 °C, the reaction between Te$_2$ vapor and Si can form SiTe (g) under our CVD conditions, which then transports to different places inside the growth chamber.[30] The as-formed SiTe (g) can react with Te$_2$ (g) and form Si$_2$Te$_3$ on the SiO$_2$/Si substrate.[28,31] When the synthesis is finished and the system is cooled down, red deposits are observed in other regions such as on the inner wall of the quartz tube around the edge of the heating zone, which indicate the formation of Si$_2$Te$_3$ at those locations. Te$_2$ vapor condenses into liquid during the cooling process. The Te$_2$ liquid pool can react with the as-formed SiTe (g) and initiates the formation of Si$_2$Te$_3$ through a vapor–liquid–solid growth process.[28] Meanwhile, the Si$_2$Te$_3$ in the liquid Te pool becomes the seed for liquid Te to condense into a solid during the cooling down process. This is seen most clearly when we have the samples in the overlapped geometry: since the gap between the two substrates is very narrow, the SiTe and Te$_2$ vapors are trapped there with a high local concentration in this narrow gap region. During the cooling process, the high-concentration Te$_2$ vapor in the gap region condenses into Te liquid, thereby providing a liquid pool for the formation of Si$_2$Te$_3$, and the as-formed Si$_2$Te$_3$ further nucleates the Te condensation.
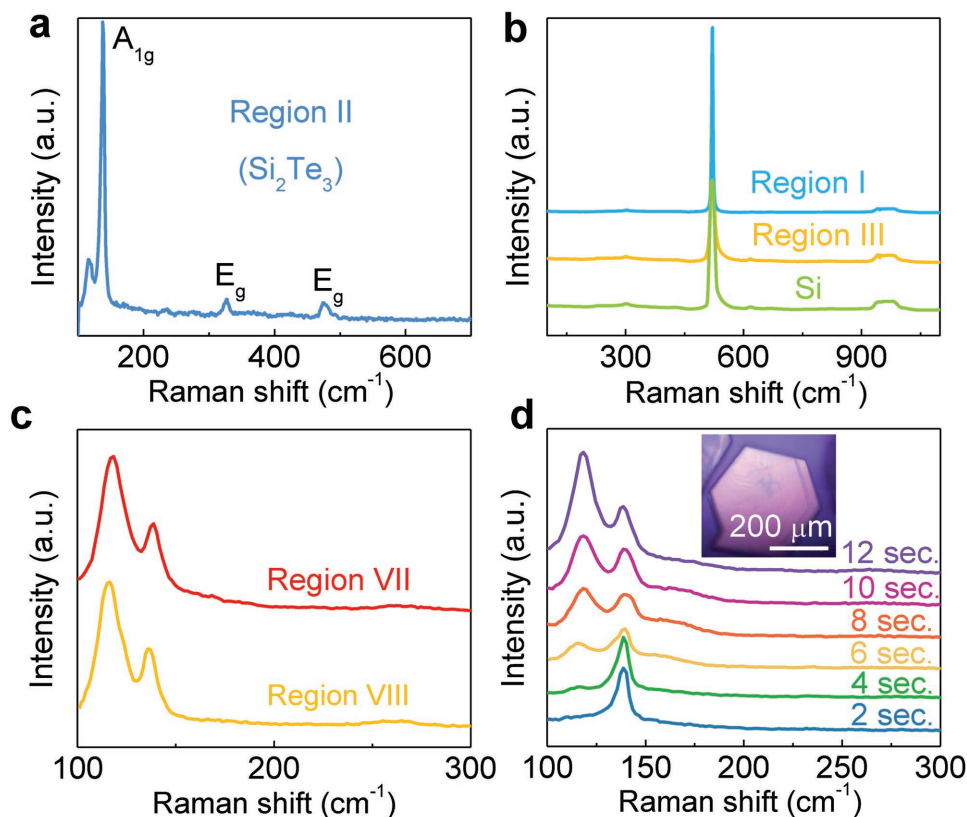
Figure 3. a) The Raman spectrum of Region II. b) Raman spectra of Region I, Region III, and a standard Si sample. c) Raman spectra of particles in regions VII and VIII. d) Time evolution of the Raman spectra of Si_2Te_3 in region II. Inset: optical microscope image of a red hexagonal Si_2Te_3 flake.

Therefore, solid Te forms together with the red Si_2Te_3 between the overlapped region during the cooling process. As a result, the two substrates are usually found to stick to each other. For the uncovered region (Region I), the concentration of SiTe and Te_2 should be much lower, and only some particles were observed on the surface of the uncovered region (Figure 2f). In the Raman spectrum of the particles, the peak of 118 cm^{-1} has strong intensity with a smaller intensity peak at 137 cm^{-1} (Figure 3c), which can be attributed to the evolution products of Si_2Te_3 (Figure 3a). During the cooling process, red Si_2Te_3 also appears on the inner wall of the quartz tube (Figure 1d) around the edge of the heating zone. It is likely that a portion of the SiTe transported downstream with the gas flow and formed Si_2Te_3 with the condensed liquid Te on the quartz tube.

We found that the as-formed Si_2Te_3 is very unstable in air, especially under the laser illumination. The time evolution of Raman spectra of Si_2Te_3 is shown in Figure 3d. The Raman spectrum of the as-formed Si_2Te_3 shows only one peak at 137 cm^{-1} (2 s illumination). As the illumination time is prolonged, a new small peak appears at 118 cm^{-1}. The 118 cm^{-1} peak is gradually enhanced, while the peak at 137 cm^{-1} is suppressed with progressing time (Figure 3d). The Raman spectra of particles on the uncovered region (region VII and region VIII in Figure 3c) are similar to the Raman spectrum of Si_2Te_3 after a 12 s laser illumination time (Figure 3d). Since the Raman signal from the small particles is weak and takes a longer time to collect for the Raman spectrum in Figure 3c, the

evolution products of the particles have the same Raman peaks as Si_2Te_3 after laser illumination. Besides the Si_2Te_3 particles, other parts of the uncovered region on sample 1 (Region I) and unoverlapped sample 2 (Region III) show only Si signal in their Raman spectra (Figure 3b). This indicates that no $MoTe_2$ is synthesized for both the overlapped and the uncovered geometry without molecular sieves. Previous works have demonstrated that Te reacts easily with Si and that the time for the Te and Si reaction is relatively short.[28,30] It is likely that during the whole 60 min reaction at 700 °C, the Te reacts with Si, and the MoO_x precursor is gradually lost by evaporation.

By contrast, when molecular sieves were introduced into the CVD growth system, the situation is found to be completely different. No Si_2Te_3 was detected on either the substrate or the inner wall of the quartz tube. In addition, 2H and 1T′ $MoTe_2$ can be successfully synthesized on the same substrate with a one-step CVD growth process using the overlapped geometry, as shown in sample 3. As seen in Figure 2d, the boundary between the uncovered and overlapped part in sample 3 can be clearly observed because the 1T′ and 2H phases show different optical contrast. Both uncovered (region IV) and covered areas (region V) of sample 3 were characterized by Raman spectroscopy, as shown in **Figure 4**a. The characteristic peaks of 1T′ $MoTe_2$, A_g (107 cm^{-1}), A_g (127 cm^{-1}), A_g (161 cm^{-1}), and A_g (256 cm^{-1}) were observed for the whole uncovered region (Region IV in Figure 2d).[17] By contrast, the Raman spectrum of the covered region
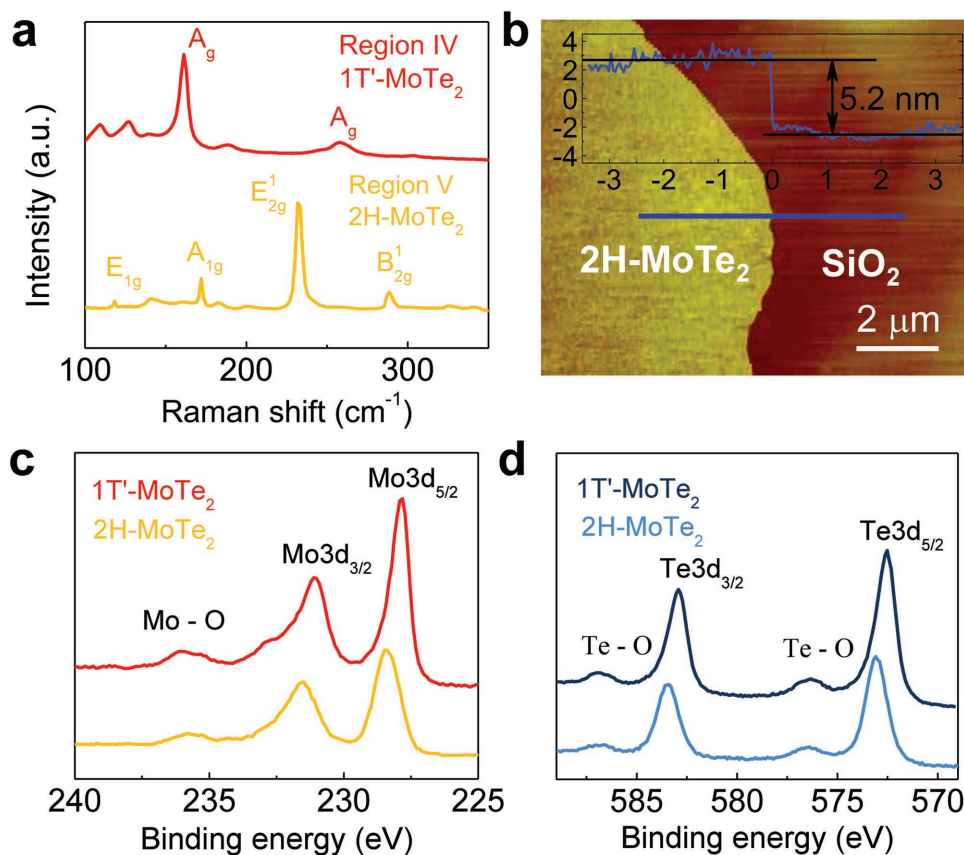
Figure 4. a) Raman spectra of the 1T′ MoTe$_2$ film (red) and 2H MoTe$_2$ (yellow). b) An AFM image of the CVD-grown 2H MoTe$_2$ sample. The height profile (inset) indicates that the as-grown film has a thickness of ≈5.2 nm. c) XPS spectra of the Mo 3d core levels for the CVD-grown 1T′ MoTe$_2$ film (red) and the 2H MoTe$_2$ film (yellow). d) High-resolution XPS Te 3d spectra of the same region on the CVD-grown 1T′ MoTe$_2$ film (blue-black) and the 2H MoTe$_2$ film (blue).

(region V in Figure 2d) indicates the characteristic peaks of few-layer 2H MoTe$_2$. The Raman spectrum shows a prominent peak of the in-plane E$_{2g}$ mode at ≈232 cm^{-1}, with a small out-of-plane A$_{1g}$ peak at ≈172 cm^{-1} and the in-plane E$_{1g}$ mode at ≈118 cm^{-1} (Figure 4a). It is noteworthy that there is a strong B$_{2g}$ peak at ≈291 cm^{-1}, which indicates that the as-grown 2H MoTe$_2$ should be few-layer 2H MoTe$_2$. According to the previous report, this peak cannot be observed in the bulk crystals, and the intensity is enhanced with decreasing thickness.[32]

To evaluate the boundary of the 1T′ MoTe$_2$ and 2H MoTe$_2$ film, micro-Raman mapping was performed. The Raman intensity map shows that 1T′ MoTe$_2$ (Figure S1b, Supporting Information) and 2H MoTe$_2$ (Figure S1c, Supporting Information) do not have a sharp boundary. On the covered part, the pure 2H MoTe$_2$ appears at about 50 μm away from the boundary line. On the uncovered part, it appears that there is a region of 1T′ and 2H MoTe$_2$ mixture from the boundary line to nearly 150 to 200 μm away. For the region 200 μm away from the boundary, it is pure 1T′ MoTe$_2$.

The atomic force microscopy (AFM) image of the grown film on the edge (Figure 4b) reveals that the 2H MoTe$_2$ is a continuous thin film, with a height of ≈5.2 nm. The 2H MoTe$_2$ surface has a roughness of ≈0.7 nm. Since the interlayer spacing in MoTe$_2$ is about 0.7 nm,[18] the number of the layers

of the as-prepared film should be ≈7. These results indicate that the 2H MoTe$_2$ and 1T′ MoTe$_2$ films have been successfully synthesized on the same SiO$_2$/Si substrate within 60 min through one-step tellurization process.

X-ray photoelectron spectroscopy (XPS) was utilized to detect the elemental composition and bonding types of these CVD-grown films. For the high resolution Mo 3d spectra of 1T′ MoTe$_2$ and 2H MoTe$_2$, the prominent Mo 3d$_{5/2}$ peaks appear at 227.9 and 228.4 eV, and the Mo 3d$_{3/2}$ peaks at 231.1 and 231.6 eV are assigned to Mo—Te bonds in 1T′ and 2H MoTe$_2$, respectively (Figure 4c). The weak peaks of 232.8 and 236.0 eV correspond to Mo—O bonds. The Te 3d$_{5/2}$ peaks of 1T′ and 2H MoTe$_2$ located at 572.5 and 573 eV, and the Te 3d$_{3/2}$ of 1T′ and 2H MoTe$_2$ located at 582.9 and 583.4 eV, respectively, are attributed to Mo—Te bonds (Figure 4d).[17,33] The energy shifts of the 2H and 1T′ MoTe$_2$ are supposed to be due to the different lattice symmetry. The small peaks of 576.4 and 587.0 eV correspond to the Te—O impurity.[33] The small shoulder peaks of Mo—O and Te—O may come from the oxidation products of MoTe$_2$ because MoTe$_2$ oxidizes easily in air.

For the sample with the MoO$_x$ layer facing down with uncovered geometry (sample 4 in Figure 2), only 1T′ MoTe$_2$ can be synthesized after tellurization while using molecular sieves. This result is similar to the uncovered part of sample 3 in the

**ADVANCED
FUNCTIONAL
MATERIALS**

www.afm-journal.de

**ADVANCED
SCIENCE NEWS**

www.advancedsciencenews.com

FULL PAPER

overlapped geometry (Region IV in Figure 2e). Meanwhile, the overlapping edges coincide with the boundary of 2H and 1T' $MoTe_2$. These phenomena indicate that the overlapped geometry played a crucial role in the growth of either 2H or 1T' $MoTe_2$.

The possible reason for the formation of 2H $MoTe_2$ in the overlapped region could be that a high concentration Te_2 vapor is maintained in the gap of the covered region. At high temperature ($T > 450 °C$), Te vaporizes and transports to every location inside the reaction zone, including the gap between the overlapped samples. Because it is difficult to blow away the Te_2 vapor in the gap between the two covered parts, the Te_2 vapor accumulates in the overlapped region during the growth. And it is possible that the high concentration Te_2 vapor and the longer residence time assist the growth of 2H $MoTe_2$.[20,34]

To better understand the role of molecular sieves for the synthesis of $MoTe_2$, we characterized the molecular sieves before and after the CVD synthesis. **Figure 5**a,b are photographs of the molecular sieves in the crucible before and after the CVD
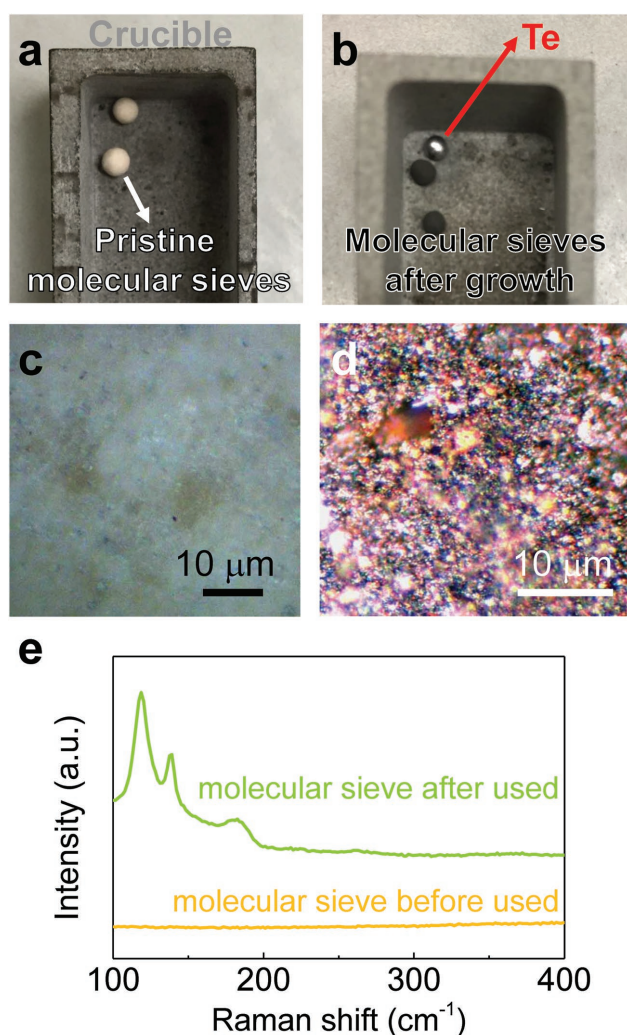
Figure 5. a,b) Photograph of molecular sieves in a crucible (a) before and (b) after $MoTe_2$ growth. c,d) The optical microscope images of a molecular sieve's surface (c) before and (d) after $MoTe_2$ growth. e) The Raman spectrum of a molecular sieve before and after the CVD synthesis.

synthesis. It can be seen from Figure 5b that after the growth, the molecular sieves changed in color from white to black, and a small amount of silvery Te solid ball remains in crucible. The black color of molecular sieves suggests the coating of Te on them. Typically, molecular sieves have a strong adsorption capacity and can adsorb byproducts like SiTe and Si_2Te_3, which are generated during the CVD synthesis. It can be anticipated that during the growth, the molecular sieves can also adsorb a great amount of SiTe and Te_2 vapors. The adsorbed SiTe and Te molecules can form Si_2Te_3 on the inner wall and surface of the molecular sieve. Figure 5c,d shows the optical microscope images of the surface of molecular sieves before and after the CVD synthesis. After the growth, red and black particles appear on the molecular sieve surface (Figure 5d), in strong contrast with the optical image of the clean surface of the sieve before the growth (Figure 5c). To study the components of these emerging particles on molecular sieves, Raman spectra were taken. Figure 5e shows the Raman spectrum of the as-obtained red material. Two strong peaks appear at 118 and 137 cm^{-1}, which are the characteristic peaks of the evolution product of Si_2Te_3. It appears that with the presence of molecular sieves, SiTe is confined to molecular sieves only (and SiTe or Si_2Te_3 no longer appear on the surface of the growth substrate or the quartz tube wall). Moreover, Te on the molecular sieves can react with SiTe to form Si_2Te_3. As a result, with the help of molecular sieves, Te_2 can react with the MoO_x on the surface of the substrate. It can be anticipated that this method could be used in the synthesis of other telluride-based layered materials (such as WTe_2, GaTe) on Si substrate without interference from the side reaction.

It was found that the amount of molecular sieves is important to the synthesis of $MoTe_2$. If the molecular sieves are insufficient and cannot completely adsorb the byproduct, a small amount of Si_2Te_3 will be found on the samples. It was also found that the growth conditions of 2H and 1T' $MoTe_2$ will be changed if too many molecular sieves are added to the CVD system.

Different adsorbents were utilized in the CVD synthesis of $MoTe_2$ to further investigate the mechanism of the molecular sieves' adsorption. **Table 1** provides a summary of different adsorbents, formulae, and the corresponding growth results in the synthesis of $MoTe_2$. Molecular sieves with different formulae and various pore diameters all show good adsorption of silicon telluride. By contrast, it was found that activated carbon powder or Al_2O_3, TiO_2, SiO_2 nanoparticle powders cannot effectively adsorb the byproducts, and Si_2Te_3 was formed on the samples.

We suspect the differences lie in several features of the molecular sieves. First, the molecular sieve preferentially adsorbs polar molecules. Second, it not only has a high adsorption capability, its structure allows the adsorbed molecules to be trapped inside even at high temperatures. Therefore, even though active carbon has a large specific surface area (≈ 1000 m^2 g^{-1}), it is nonpolar and thus may have a low affinity for polar molecules like SiTe. Furthermore, at the growth temperature (700 °C), desorption can easily occur, whereas in the case of molecular sieves, due to the small pore structure, the adsorbed molecules can be trapped at this temperature. For the case of Al_2O_3, TiO_2, and SiO_2 nanoparticle powders, although

**ADVANCED
SCIENCE NEWS**

www.advancedsciencenews.com

**ADVANCED
FUNCTIONAL
MATERIALS**

www.afm-journal.de

FULL PAPER

Table 1. Summary of adsorbent, formula, and the growth results in the synthesis of $MoTe_2$.

Adsorbent	Formula	Growth results
3 Å molecular sieves	$K_nNa_{12-n}[(AlO_2)_{12}(SiO_2)_{12}] \cdot x\,H_2O$	$MoTe_2$ grown on SiO_2/Si substrate
		No red pollutant
4 Å molecular sieves	$Na_{12}[(AlO_2)_{12}(SiO_2)_{12}] \cdot x\,H_2O$	$MoTe_2$ grown on SiO_2/Si substrate
		No red pollutant
5 Å molecular sieves	$Ca_nNa_{12-2n}[(AlO_2)_{12}(SiO_2)_{12}] \cdot x\,H_2O$	$MoTe_2$ grown on SiO_2/Si substrate
		No red pollutant
13× (10 Å) molecular sieves	$Na_{86}[(AlO_2)_{86}(SiO_2)_{106}] \cdot x\,H_2O$	$MoTe_2$ grown on SiO_2/Si substrate
		No red pollutant
Activated carbon powder	C	Red pollutant on SiO_2/Si substrate
Al_2O_3 nano-particle powder	Al_2O_3	Red pollutant on SiO_2/Si substrate
TiO_2 nano-particle powder	TiO_2	Red pollutant on SiO_2/Si substrate
SiO_2 nano-particle powder	SiO_2	Red pollutant on SiO_2/Si substrate

they have an affinity to adsorb polar molecules, they do not have pores that are comparable to the size of the adsorbed molecules to trap them.

3. Conclusions

In summary, we have found that molecular sieves can adsorb byproduct silicon telluride and can eliminate the influence of the side reaction during the CVD synthesis of $MoTe_2$. Without molecular sieves, only Si_2Te_3 instead of $MoTe_2$ was obtained. With the help of molecular sieves, few-layer $MoTe_2$ can be synthesized on the SiO_2/Si substrate without disturbance from the side reaction. 1T′ $MoTe_2$ can be grown directly from the MoO_x precursor. Pure 1T′ $MoTe_2$ and 2H $MoTe_2$ regions synthesized on the same piece of SiO_2/Si substrate can also be obtained by using an overlapped geometry. Even though the studies in this work focus on the synthesis of $MoTe_2$, the same strategy could potentially be extended to the synthesis of other tellurium-based layered materials.

Supporting Information

Supporting Information is available from the Wiley Online Library or from the author.

Acknowledgements

[1] A. K. Geim, K. S. Novoselov, *Nat. Mater.* **2007**, *6*, 183.
[2] V. Nicolosi, M. Chhowalla, M. G. Kanatzidis, M. S. Strano, J. N. Coleman, *Science* **2013**, *340*, 1226419.
[3] K. S. Novoselov, A. K. Geim, S. V. Morozov, D. Jiang, M. I. Katsnelson, I. V. Grigorieva, S. V. Dubonos, A. A. Firsov, *Nature* **2005**, *438*, 197.
[4] B. Radisavljevic, A. Radenovic, J. Brivio, V. Giacometti, A. Kis, *Nat. Nano* **2011**, *6*, 147.
[5] X. Qian, J. Liu, L. Fu, J. Li, *Science* **2014**, *346*, 1344.
[6] X. Huang, Z. Zeng, H. Zhang, *Chem. Soc. Rev.* **2013**, *42*, 1934.
[7] Q. H. Wang, K. Kalantar-Zadeh, A. Kis, J. N. Coleman, M. S. Strano, *Nat. Nano* **2012**, *7*, 699.
[8] R. Lv, J. A. Robinson, R. E. Schaak, D. Sun, Y. Sun, T. E. Mallouk, M. Terrones, *Acc. Chem. Res.* **2015**, *48*, 56.
[9] A. Splendiani, L. Sun, Y. Zhang, T. Li, J. Kim, C.-Y. Chim, G. Galli, F. Wang, *Nano Lett.* **2010**, *10*, 1271.
[10] L. Zhang, A. Zunger, *Nano Lett.* **2015**, *15*, 949.
[11] M. N. Ali, J. Xiong, S. Flynn, J. Tao, Q. D. Gibson, L. M. Schoop, T. Liang, N. Haldolaarachchige, M. Hirschberger, N. P. Ong, R. J. Cava, *Nature* **2014**, *514*, 205.
[12] K.-A. N. Duerloo, Y. Li, E. J. Reed, *Nat. Commun.* **2014**, *5*, 4214.
[13] Y. Qi, P. G. Naumov, M. N. Ali, C. R. Rajamathi, W. Schnelle, O. Barkalov, M. Hanfland, S.-C. Wu, C. Shekhar, Y. Sun, V. Susz, M. Schmidt, U. Schwarz, E. Pippel, P. Werner, R. Hillebrand, T. Forster, E. Kampert, S. Parkin, R. J. Cava, C. Felser, B. Yan, S. A. Medvedev, *Nat. Commun.* **2016**, *7*, 11038.
[14] C. Ruppert, O. B. Aslan, T. F. Heinz, *Nano Lett.* **2014**, *14*, 6231.
[15] H. D. Abruña, G. A. Hope, A. J. Bard, *J. Electrochem. Soc.* **1982**, *129*, 2224.
[16] D. H. Keum, S. Cho, J. H. Kim, D.-H. Choe, H.-J. Sung, M. Kan, H. Kang, J.-Y. Hwang, S. W. Kim, H. Yang, K. J. Chang, Y. H. Lee, *Nat. Phys.* **2015**, *11*, 482.
[17] L. Zhou, K. Xu, A. Zubair, A. D. Liao, W. Fang, F. Ouyang, Y.-H. Lee, K. Ueno, R. Saito, T. Palacios, J. Kong, M. S. Dresselhaus, *J. Am. Chem. Soc.* **2015**, *137*, 11892.
[18] Y.-F. Lin, Y. Xu, S.-T. Wang, S.-L. Li, M. Yamamoto, A. Aparecido-Ferreira, W. Li, H. Sun, S. Nakaharai, W.-B. Jian, K. Ueno, K. Tsukagoshi, *Adv. Mater.* **2014**, *26*, 3263.
[19] I. G. Lezama, A. Arora, A. Ubaldini, C. Barreteau, E. Giannini, M. Potemski, A. F. Morpurgo, *Nano Lett.* **2015**, *15*, 2336.
[20] S. Cho, S. Kim, J. H. Kim, J. Zhao, J. Seok, D. H. Keum, J. Baik, D.-H. Choe, K. J. Chang, K. Suenaga, S. W. Kim, Y. H. Lee, H. Yang, *Science* **2015**, *349*, 625.
[21] Z. H. Ni, H. M. Wang, J. Kasim, H. M. Fan, T. Yu, Y. H. Wu, Y. P. Feng, Z. X. Shen, *Nano Lett.* **2007**, *7*, 2758.
[22] H. Li, J. Wu, X. Huang, G. Lu, J. Yang, X. Lu, Q. Xiong, H. Zhang, *ACS Nano* **2013**, *7*, 10344.
[23] Y.-H. Lee, X.-Q. Zhang, W. Zhang, M.-T. Chang, C.-T. Lin, K.-D. Chang, Y.-C. Yu, J. T.-W. Wang, C.-S. Chang, L.-J. Li, T.-W. Lin, *Adv. Mater.* **2012**, *24*, 2320.

FULL PAPER

[24] X. Wang, H. Feng, Y. Wu, L. Jiao, *J. Am. Chem. Soc.* **2013**, *135*, 5304.

[25] X. Wang, Y. Gong, G. Shi, W. L. Chow, K. Keyshar, G. Ye, R. Vajtai, J. Lou, Z. Liu, E. Ringe, B. K. Tay, P. M. Ajayan, *ACS Nano* **2014**, *8*, 5125.

[26] A. L. Elías, N. Perea-López, A. Castro-Beltrán, A. Berkdemir, R. Lv, S. Feng, A. D. Long, T. Hayashi, Y. A. Kim, M. Endo, H. R. Gutiérrez, N. R. Pradhan, L. Balicas, T. E. Mallouk, F. López-Urías, H. Terrones, M. Terrones, *ACS Nano* **2013**, *7*, 5235.

[27] C. Huang, S. Wu, A. M. Sanchez, J. J. P. Peters, R. Beanland, J. S. Ross, P. Rivera, W. Yao, D. H. Cobden, X. Xu, *Nat. Mater.* **2014**, *13*, 1096.

[28] S. Keuleyan, M. Wang, F. R. Chung, J. Commons, K. J. Koski, *Nano Lett.* **2015**, *15*, 2285.

[29] S. Chuang, C. Battaglia, A. Azcatl, S. McDonnell, J. S. Kang, X. Yin, M. Tosun, R. Kapadia, H. Fang, R. M. Wallace, A. Javey, *Nano Lett.* **2014**, *14*, 1337.

[30] R. F. Brebrick, *J. Chem. Phys.* **1968**, *49*, 2584.

[31] L. G. Bailey, *J. Phys. Chem. Solids* **1966**, *27*, 1593.

[32] M. Yamamoto, S. T. Wang, M. Ni, Y.-F. Lin, S.-L. Li, S. Aikawa, W.-B. Jian, K. Ueno, K. Wakabayashi, K. Tsukagoshi, *ACS Nano* **2014**, *8*, 3895.

[33] J. C. Bernède, C. Amory, L. Assmann, M. Spiesser, *Appl. Surf. Sci.* **2003**, *219*, 238.

[34] L. Zhou, A. Zubair, Z. Wang, X. Zhang, F. Ouyang, K. Xu, W. Fang, K. Ueno, J. Li, T. Palacios, J. Kong, M. S. Dresselhaus, *Adv. Mater.*, **2016**, DOI:10.1002/adma.201602687.